Mg-doping threshold effect and H-containing defects in $LiNbO_3$

1993 J. Phys.: Condens. Matter 5 2423

(http://iopscience.iop.org/0953-8984/5/15/013)

J. Phys.: Condens. Matter 5 (1993) 2423–2430. Printed in the UK

Mg-doping threshold effect and H-containing defects in $LiNbO_3$

Xi-Qi Feng† and Tong B Tang‡

† Shanghai Institute of Ceramics, Academia Sinica, Shanghai 200050, People's Republic of China

‡Physics Department, Hong Kong Baptist College, Kowloon Tong, Kowloon, Hong Kong

Received 7 July 1992, in final form 11 November 1992

Abstract. The OH infrared absorption spectra of heavily Mg-doped $LiNbO_3$ codoped with a trivalent or a divalent cation impurity have been investigated, and some correlated with ESR measurements. We examine how the threshold effect in Mg doping determines the incorporation sites of the codopant and attempt to derive a general relationship between impurity lattice sites and the OH spectrum. A main absorption band that peaked at 3536 cm^{-1} appeared in all the samples and is attributed to OH stretching vibration in the Mg_{Li}–OH–Mg_{Nb} complex. Those codoped with M^{3+} (M ≡ Fe, Cr, Nd) exhibited additional OH bands within the 3500–3525 cm^{-1} range, the actual peak position depending on the charge misfit and the ionic radius of the impurity cation. They are attributed to Mg_{Li}–OH–Me^{3+}_{Nb} complexes. We did not find any additional band for M^{3+} ≡ Er^{3+}, Ho^{3+}, Tm^{3+}. A simple scheme is proposed that depicts whether such a new feature should appear, depending on the ionic radius and the electronegativity of the trivalent ion. We observed no change in either the infrared or the ESR spectrum in the case of a Tr^{2+} codopant (Tr ≡ Co, Ni or Cu), implying that its lattice site is unaffected by Mg doping.

1. Introduction

There has been growing interest in the last decade to understand the basic physics of the threshold effect in the Mg doping of $LiNbO_3$. The importance of Mg stems from the observation by Zhong *et al* (1980) that the resistance to optical damage is improved a hundredfold in congruent $LiNbO_3$ when 4.6 mol% MgO has been added to the melt. In the absence of photorefraction, light wave fronts may then propagate without distortion in electro-optical devices fabricated from this material. Bryan *et al* (1984) and Sweeney *et al* (1985) confirmed the observation and showed that this effect exhibits a distinct threshold at a critical Mg impurity level, and that additionally several other properties suffer sharp changes when the threshold is exceeded. Undoubtedly, such a threshold phenomenon marks some profound change in the lattice environment. This change is the appearance of Mg_{Nb} defects, as proposed by Feng *et al* (1988a) and Zhang and Feng (1990) based on considerations of the lattice structure and the defect chemistry of lithium niobate. Accordingly, they calculated that the threshold concentration of Mg should be 5.3 mol% for the congruent melt. This predicted threshold is in quantitative agreement with observed transitions in the optical absorption edge, OH infrared absorption bands and lattice parameters for samples with increasing dopant levels (Feng *et al* 1990c). Moreover, direct NMR measurements on Mg in the samples revealed that its spectral linewidth and symmetry similarly display the threshold effect, at 5–6 mol% (Feng *et al* 1988b, 1990b). Computationally, Donnerberg *et al* (1992) study the incorporation of divalent and trivalent cations into the $LiNbO_3$ lattice and affirm

0953-8984/93/152423+08$07.50

that Mg^{2+} in excess of a threshold concentration would separately occupy both Nb and Li sites. Mg_{Nb} defects have also been implied by Grabmaier *et al* (1991).

The threshold effect highlights the strong dependence of extrinsic defects on intrinsic defects in lithium niobate. Li^{+} and Nb^{5+} have almost identical sizes and lattice environments (distorted octahedra formed by six O^{2-}) and hence a tendency to large non-stoichiometry; for crystals grown from a congruent melt, [Li]/[Nb] = 0.942. Charge compensation demands therefore a high concentration of intrinsic defects. The unusual property of Mg dopant will significantly affect which lattice sites other foreign ions may enter into. In this paper, we aim to elucidate the influence of the threshold effect on the choice of sites by divalent and trivalent impurity cations, as well as the associated charge compensation mechanisms.

Our starting point will be an experimental examination of how the OH absorption spectra change with trivalent codopants in $LiNbO_3$:Mg. As-grown crystals of lithium niobate, as in the case of many other perovskites such as strontium titanate, always contain hydrogen, but the stretching vibration band of the resulting hydroxyl ions in the vicinity of 3500 cm^{-1} often shows features and is broader by an order of magnitude (Schirmer 1991). Its position, shape, linewidth and polarization characteristics reflect sensitively the ionic environment in the lattice; it may indeed serve as a probe into the defect structure (Feng *et al* 1988b). We shall in this paper compare known data from $LiNbO_3$:Mg, M^{3+} (M ≡ Fe, Cr, Nd and Er) with our own results and also report new data from $LiNbO_3$ codoped with Mg, Re^{3+} (Re ≡ Ho and Tm) or Mg, Tr^{2+} (Tr ≡ Co, Ni and Cu). Besides these OH spectra, ESR experiments have also been performed, to obtain more information about the lattice siting of specific impurities. A unified interpretation will then be given, and conclusions drawn regarding some aspects of the interaction between intrinsic and extrinsic defects, which is eventually responsible for the abrupt changes in certain optoelectronic properties of $LiNbO_3$. The last phenomena demand serious attention, if only for practical reasons.

2. Experimental details

All the samples used in this work were grown in a Czochralski furnace, with pulling along the *c* axis and a melt of 99.9% pure Nb(V) oxide and Li carbonate, in congruent composition. 6 mol% Mg oxide or other dopants or both were added as appropriate. $LiNbO_3$ doped thus was more difficult to grow and pole than the pure compound; the resulting crystals exhibited a large number of regularly distributed inclusions and growth streaks visible to the naked eye. Samples were then cut from sections of good optical quality. Table 1 lists the impurity levels in these samples.

Table 1. Melt-doped samples.

Sample	1	2	3	4	5	6	7	8
Li–Nb (melt)	0.945	0.945	0.945	0.945	0.945	0.945	0.945	0.945
MgO (melt) (mol%)	6.0	—	6.0	6.0	6.0	6.0	6.0	6.0
Fe_2O_3 (crystal) (ppm)[a]	—	650	530	—	—	—	—	—
Cr_2O_3 (melt) (mol%)	—	—	—	0.5	—	—	—	—
Nd_2O_3 (melt) (mol%)	—	—	—	—	0.5	—	—	—
Er_2O_3 (melt) (mol%)	—	—	—	—	—	0.5	—	—
Ho_2O_3 (melt) (mol%)	—	—	—	—	—	—	0.5	—
Tm_2O_3 (melt) (mol%)	—	—	—	—	—	—	—	0.5

[a] Fe concentration determined with AA.

Doping with Tr (≡ Cu, Co and Ni) was achieved by closed-ampoule diffusion. Undoped $LiNbO_3$ powder mixed with CuO, CoO or NiO served as the source material, and the diffusion temperature was set at 900 °C (Cu) or 1050 °C (Co and Ni) (table 2).

Table 2. Diffusion-doped samples.

Sample	9	10	11	12	13	14
Li–Nb (melt)	0.945	0.945	0.945	0.945	0.945	0.945
MgO (melt) (mol%)	—	6.0	—	6.0	—	6.0
Dopants	CoO[a]	CoO	NiO	NiO	CuO	CuO

[a] Added to the melt.

Room-temperature spectra of the OH vibration were taken with a Nicolet 7000 FTIR spectrometer, which offered a resolving power of better than 2 cm^{-1}. Their polarization dependence was obtained by incorporation of a silver bromide grating. Visible-light absorption used as a measure of impurity level was determined with a Beckman 5270 instrument. ESR experiments on some samples were performed on a JES-FEIXG spectrometer, at room temperature and with the magnetic field parallel to their *c* axis.

3. Results

Figure 1 depicts the OH absorption in $LiNbO_3$ doped with 6 mol% Mg, which peaks at 3536 cm^{-1} and has a finite component along the *c* axis. It shows up in all heavily Mg-doped samples whether codoped or not. This shift in peak position from its usual location at 3484 cm^{-1} as a consequence of the threshold effect was first observed by Bryan *et al* (1984), and Feng *et al* (1988b, 1990c) have found that the Mg threshold level occurred between 5% and 6% in the congruent melt. The absorption band was assigned by Kovács *et al* (1988) to an OH vibration in the Mg–OH complex and, according to Feng *et al* (1988b, 1990c), attributed to Mg at Nb sites and should thus be labelled as the Mg_{Nb}–OH band.

An extra absorption band at 3504 cm^{-1} appeared in (Mg, Fe)-codoped samples, which, as figure 2 indicates, vanished when the electric field vector of radiation aligned with their *c* axis, implying that the OH dipole responsible lies in the oxygen plane. We prepared a sample, 25 mm high in the direction of the *c* axis, along with the Fe doping level increased gradually from bottom to top. Comparison with the intensity of the 482 nm absorption peak that corresponds to the spin-forbidden d–d transition in Fe^{3+}, and which is therefore proportional to the doping level, proved that the absorption coefficient for 3504 cm^{-1} was proportional to the iron concentration. The feature at 3504 cm^{-1} looks as if it is independent of the vibration mode at 3536 cm^{-1}.

Figure 3 shows the OH absorption and its polarization characteristics for $LiNbO_3$: Mg, Cr. The additional band at 3506 cm^{-1} has also been reported by Kovács *et al* (1988), but their samples had [Li]/[Nb] = 1.1 and 4 mol% Mg, as well as a greatly different Cr concentration of 0.035%.

Let us now turn to the data for rare earths. When Nd was codoped, the width at half-maximum of the OH band at 3536 cm^{-1} increases from 40 to 48 cm^{-1}, indicative of an unresolved OH band close to the 3536 cm^{-1} band, on the small-wavenumber side. This agrees with the proposal of Kovács *et al* (1990) that Mg^{2+}–OH–Nd^{3+} defects give rise to an absorption band at 3522 cm^{-1}. The band should show up more distinctively with higher Nd doping. On the other hand, the polarized OH bands in samples codoped with Er (sample 6), with Ho (sample 7) and with Tm (sample 8) have a similar appearance to that in figure

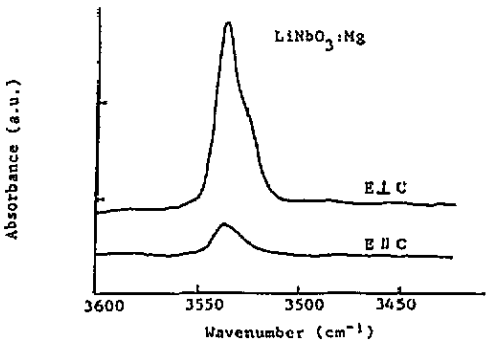

Figure 1. Polarized OH absorption band in heavily Mg-doped $LiNbO_3$, i.e. sample 1.

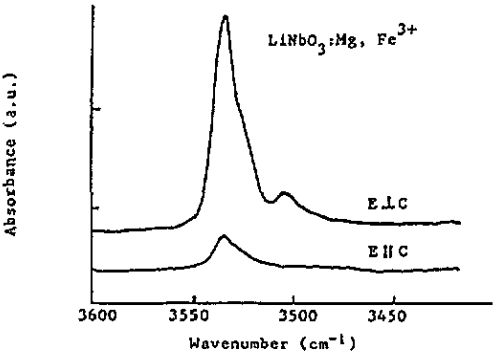

Figure 2. Polarized OH absorption band in $LiNbO_3$:Mg, Fe, i.e. sample 3.

1. This absence of any new feature, an experimental finding in this work, is in the case of Er codoping consistent with the deduction of Kovács *et al* (1991) who, based on evidence from Rutherford back scattering, deduced that Er substitutes for Li, that Er_{Nb} defects are not formed and that no new OH band therefore appears within 3500–3525 cm^{-1}.

The spectra in the cases of codoping with Tr^{2+} (Tr ≡ Co, Ni and Cu, i.e. samples 10, 12 and 14) have been obtained in this work and again found to resemble that for doping with Mg only. The 3536 cm^{-1} band exhibited variations in intensity, but its shape and polarization characteristics did not change. Table 3 is a summary of all the infrared data here discussed.

Table 3. OH bands for Mg-doped $LiNbO_3$ with various codopants.

Li–Nb + Mg doping (melt)	Codopant	Mg_{Nb}–OH–Mg_{Li} band (cm^{-1})	M_{Nb}–OH–Mg_{Li} band (cm^{-1})	Reference
0.945 + 6%	—	3536	—	This work
0.945 + 6%	530 ppm Fe^{3+}	3536	3504	This work
0.945 + 6%	0.5% Cr_2O_3	3536	3506	This work
0.945 + 6%	0.5% Nd_2O_3	3536	~3520	This work
0.945 + 6%	0.5% Er_2O_3	3536	—	This work
0.945 + 6%	0.5% Ho_2O_3	3536	—	This work
0.945 + 6%	0.5% Tm_2O_3	3536	—	This work
0.945 + 6%	CoO	3536	—	This work
0.945 + 6%	NiO	3536	—	This work
0.945 + 6%	CuO	3536	—	This work
0.945 + 5%	0.1% Fe_2O_3	3537	3507	de Rosendo *et al* (1986)
1.1 + 4%	0.035% Cr_2O_3	3539	3506	Kovács *et al* (1988)
0.945 + 6%	2% Nd_2O_3	3538	3522	Kovács *et al* (1990)
0.945 + 5.8%	0.5% Er_2O_3	3538	—	Kovács *et al* (1991)
0.945 + 6%	0.5% TiO_2	3538	—	Kovács *et al* (1990)
0.945 + 6%	0.1% MnO	3538	—	Kovács *et al* (1990)

ESR spectroscopy of the impurity ions may lead to further information concerning the lattice sites that they occupy. Measurements under liquid-nitrogen temperature provided evidence that Fe^{3+} entered new sites as a result of high Mg doping (Sweeney *et al* 1985). A similar observation has been made at room temperature in $LiNbO_3$:6% MgO

plus 530 ppm Fe (sample 3) by Feng *et al* (1990a) and Böker *et al* (1990). In this codoped sample, in addition to the signal from Fe_{Li}^{3+}, a second signal was clearly present corresponding to Fe_{Nb}^{3+}. We have also measured the room-temperature ESR lines of Cu^{2+} in Mg-codoped and in singly Cu-doped $LiNbO_3$ (samples 14 and 13). These lines looked alike, both rather broad, with $g_{11} = 2.26 \pm 0.03$ in accord with previous observation (Petrosyan *et al* 1984). Fe was detected as a trace impurity. The typical Fe_{Nb}^{3+} signal could be observed in the Cu-codoped crystal, meaning that the Mg doping level there exceeded the threshold. The absence of change in the ESR spectra of Cu^{2+} implies that its site of incorporation is unaffected by the threshold effect. Generally speaking, all Tr-diffusion-doped crystals contained Fe. We have measured the ESR signals of Co^{2+} and Ni^{2+} in samples 11–14 but did not succeed in separating them from the rather intense Fe^{3+} signals.

4. Discussion

4.1. Threshold phenomenon and lattice sites of impurity ions

The mechanism underlying the threshold effect in Mg doping has been examined by Feng *et al* (1988a) and Donnerberg *et al* (1992). The present study lends further support to the ideas proposed and provides more details. According to the suggested scheme, as the Mg concentration exceeds the threshold, intrinsic defects of isolated Nb_{Li} as well as the $(Nb_{Li}V_{Nb})$ complex disappear, while Mg^{2+} enter Nb and Li sites in a certain ratio, to form the charge self-compensated defect $Mg_{Li}(Mg_{Nb})_{1/3}(Nb_{Nb})_{2/3}O_3$. Every aggregate of three of these defects contains an Mg_{Nb} in addition to three Mg_{Li} and two Nb_{Nb}. The threshold effect arises from this change in defect structure, which greatly affects the charge compensation mechanisms for other impurities. Consider the case of a trivalent codopant. At low Mg concentrations, either of the following two situations arises.

(i) M^{3+} substitutes for Li, with $(Nb_{Li}V_{Nb})$ serving as charge compensator:

$$3Nb_2O_5 + M_2O_3 = 6[(M_{Li})_{1/3}(Nb_{Li}V_{Nb})_{2/3}(Nb_{Nb})_{1/3}O_3].$$

(ii) The M^{3+} charge self-compensates:

$$M_2O_3 = M_{Li}M_{Nb}O_3.$$

Above the threshold level, the possible incorporation reactions are as follows:

(a) M^{3+} self-compensation according to

$$M_2O_3 = M_{Li}M_{Nb}O_3$$

(b) M^{2+} self-compensation according to

$$Nb_2O_5 + 4MgO = 3[Mg_{Li}(Mg_{Nb})_{1/3}(Nb_{Nb})_{2/3}O_3]$$

(c) M^{3+} substitution for Nb, with Mg_{Li} as charge compensator, given by

$$Nb_2O_5 + 4MgO + M_2O_3 = 4[Mg_{Li}(M_{Nb})_{1/2}(Nb_{Nb})_{1/2}O_3]$$

(d) Mg^{2+} for Nb, with M_{Li} as charge compensator, given by

$$Nb_2O_5 + 4MgO + 3M_2O_3 = 6[M_{Li}(Mg_{Nb})_{2/3}(Nb_{Nb})_{1/3}O_3].$$

These possibilities correspond to the appearance of four kinds of dipole, namely M_{Li}–M_{Nb}, Mg_{Li}–Mg_{Nb}, Mg_{Li}–M_{Nb} and M_{Li}–Mg_{Nb}, respectively. As stated before, the first two types, as charge self-compensated defects from incorporation modes (a) and (b), are energetically favoured, once the threshold has been exceeded. However, also considered should be the valency, electronegativity and radius of the substituting ion. From the viewpoint of the charge state, although in (a) M_{Li}^{3+} may be compensated by M_{Nb}^{3+}, it is less preferred than Mg_{Li}^{2+} in (c), since Li has the charge number 1+. Regarding electronegativity, transition-metal ions Tr^{3+} such as Fe^{3+} and Cr^{3+} (of values 1.83 and 1.66, respectively) differ from Li^{+} (0.98) far more than does Mg^{2+} (1.31), and therefore the Mg_{Li}–Tr_{Nb} complex in (c) is again more likely to form. Thus, competition takes place when several impurities are present. Generally speaking, a large ionic radius and electronegativity favour Mg_{Li}–M_{Nb}. Among rare-earth Re^{3+} ions, although their ionic radii exceed those of Li^{+} (0.68 Å) and Mg^{2+} (0.66 Å), their electronegativities range from 1.1 to 1.3 and therefore the existence of Mg_{Li}–Re_{Nb} is contingent. Lastly, reaction (d) is improbable because both charge and electronegativity argue against Tr_{Li} or Re_{Li}, and mode (b) takes precedence. In summary, two situations may be met in supra-threshold (Mg, M^{3+})-codoped lithium niobate: either Mg_{Li}–Mg_{Nb} and M_{Li}–M_{Nb} or Mg_{Li}–Mg_{Nb} and Mg_{Li}–M_{Nb} pairs dominate its defect structure. In the next section, we shall discuss how these two different situations affect its OH absorption.

4.2. OH bands and incorporation sites of impurities

In $LiNbO_3$, protons with their small size have rapid diffusion and drift rates and therefore tend to accumulate near negatively charged centres. When impurities were doped or the Li to Nb ratio was changed, new charged centres would attain equilibrium and result in changed OH bands. In heavily Mg-doped niobate, Mg_{Nb} is the only electronegative centre, and the triangle of oxygen ions in the plane normal to the Mg_{Li}–Mg_{Nb} dipole is a favourable site for protons, forming a Mg_{Li}–OH–Mg_{Nb} complex as illustrated in figure 4(*a*). We may further expect the proton to be repelled from $(Mg_{Li})'$ towards $(Mg_{Nb})^{3}$, so that the OH dipole is inclined with respect to the oxygen plane and the OH band has a higher *c*-axis component. The inclination was measured to be $\alpha = 17°$ for our sample 1, near to the datum of Kovács *et al* (1987) who obtained $\alpha = 14°$ for their samples with [Li]/[Nb] = 1.1 + 4% MgO. On the other hand, the M_{Li}–M_{Nb} pair attains local charge balance and therefore does not attract protons.

In the second situation, the triangle of oxygen ions set perpendicular to the Mg_{Li}–M_{Nb} dipole is likewise a site favoured by protons (see figure 4(*b*)). The resulting Mg_{Li}–OH–M_{Nb} complex leads to a new OH band, which, as Kovács *et al* (1990) point out, appears within 3500–3525 cm^{-1}. Of course, in these samples the OH band near 3536 cm^{-1} arising from Mg_{Li}–OH–Mg_{Nb} is also present.

The case of M^{3+} codoped materials may be summarized thus: the appearance of any new OH band depends on whether Mg_{Li}–M_{Nb} pairs exist, itself an outcome of the competition between reactions (a) and (c). As discussed in the last section, the latter should be mainly decided by the ionic radius and the electronegativity of M. In figure 5 we plot these two properties for a number of trivalent ions, using numerical data from Keune (1981). Apparently, a straight line may be drawn to separate codoped samples with new OH bands from all those without, according to previous reports as well as the present work (table 3). This simple rule suggests that Mg_{Li}–M_{Nb} pairs are formed when M ≡ Ce, Pr, Pm, In and possibly also Eu. It may therefore be assessed by straightforward tests of such predictions.

In the case of a divalent transition-metal codopant, OH spectral and ESR measurements both indicated that the threshold effect does not give rise to Tr_{Nb}. The incorporation reaction

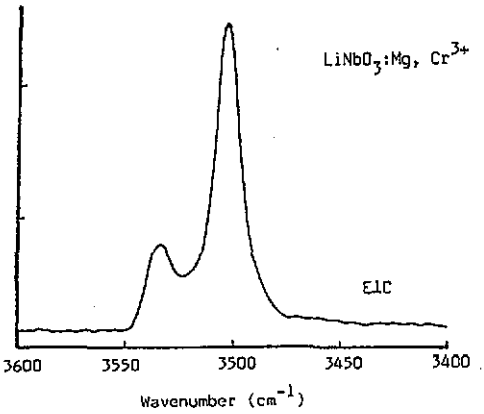

Figure 3. Polarized OH absorption band in $LiNbO_3$:Mg, Cr, i.e. sample 4.

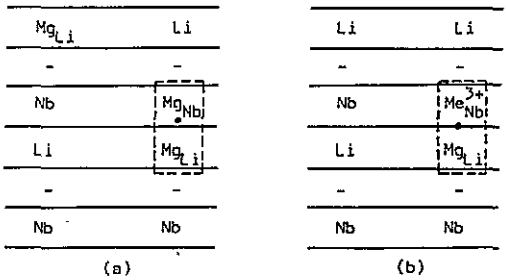

Figure 4. Schematic diagrams of the $LiNbO_3$ structure for (*a*) the Mg_{Nb}–OH–Mg_{Li} complex in heavily Mg-doped $LiNbO_3$ and (*b*) M_{Nb}–OH–Mg_{Li} complex in $LiNbO_3$:Mg, M^{3+}: –, natural vacancies in the stacking sequence; ●, protons. The horizontal lines represent close-packed oxygen planes.

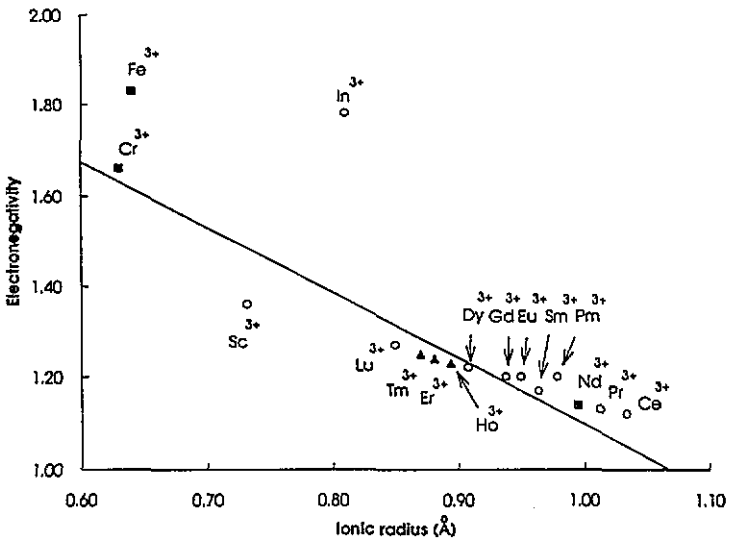

Figure 5. Ionic radii and electronegativities of codopant ions: ■, new OH band observed; ▲, none; ○, case awaiting experimental verification. The straight line separates cases with and without the new OH band.

remains as

$$Nb_2O_5 + TrO = 2[(Tr_{Li})_{1/2}(Nb_{Li}V_{Nb})_{1/2}(Nb_{Nb})_{1/2}O_3]$$

with Tr_{Li} together with Mg_{Li} serving as the charge compensator of Mg_{Nb}, to form $Tr_{Li}(Mg_{Nb})_{1/3}(Nb_{Nb})_{2/5}O_3$. Although, like Mg_{Li}–Mg_{Nb}, the Tr_{Li}–Mg_{Nb} dipole may also

accommodate an H^+ in its oxygen plane, the low concentration of Tr^{2+} (10^{-3} or less) means an indiscernible change in the OH spectrum.

4.3. Peak position of OH bands in $LiNbO_3$:Mg, M^{3+}

When the Mg concentration exceeds the threshold, some of its ions occupy Nb sites with Mg_{Li} as charge compensators. The charge number and the electronegativity of Mg are 2+ and 1.3 respectively, and 5+ and 1.6 for Nb. The Mg–O bond is therefore weaker than the Nb–O bond. Hence, where Mg replaces Nb, its neighbouring oxygen ions relax outwards. The longer O–O bonds result in a higher wavenumber for the OH stretching vibration, which explains the shift in the OH absorption peak from 3482 to 3536 cm^{-1} (Novak 1974). The increases in the oxygen octahedron volume and lattice parameters have also been independently observed (Zhang and Feng 1990).

A similar situation arises when M^{3+} replaces Nb, except that the smaller charge misfit results in a smaller increase in the O–O bond length. This probably explains why the new OH bands in $LiNbO_3$:Mg, M^{3+} all appear on the lower side of the 3536 cm^{-1} peak. Another factor of consideration should be the ionic radius of M^{3+}. A consistent trend is apparent, by which the band moves towards large wavenumbers as the radius increases.

Acknowledgments

We thank L Y Xu, L O Tang, B Y So and C B Zhu at the Institute of Ceramics for supplying the variously doped $LiNbO_3$ crystals. The work was supported by the National Science Foundation of China and the China Exchange Fund of the Hong Kong Baptist College. The FTIR spectrometer is a chemistry–physics inter-departmental facility of the College.

References

Böker A, Donnerberg H, Schirmer O F and Feng X Q 1990 *J. Phys.: Condens. Matter* **2** 6865
Bryan D A, Gerson R and Tomaschke H E 1984 *Appl. Phys. Lett.* **44** 847
Donnerberg H, Tomlinson S M, Catlow C R A and Schirmer O F 1992 *Phys. Rev.* B **44** 4877
Feng X Q, Tang L A and Ying J F 1990a *Ferroelectrics* **107** 21
Feng X Q, Wang D S and Zhang J Z 1990b *Phys. Status Solidi* b **156** K127
Feng X Q, Ying J F, Liu J C and Zhang Q R 1988a *Abstracts Int. Conf. on Defects in Insulating Crystals (Parma, 1988)* p 463
Feng X Q, Ying J F, Wang C C and Liu J C 1988b *Acta Phys. Sin.* **37** 2062
Feng X Q, Zhang Q R, Ying J F, Liu J C and Yin Z W 1990c *Sci. China* A **33** 108
Grabmaier B C, Wersing W and Koestler W 1991 *J. Crystal Growth* **110** 339
Keune H 1981 *Chimica-ein Weissensspeicher* vol 1 (Berlin: Springer) p 2
Kovács L, Földvari I, Cravero I, Polgár K and Capelletti R 1988 *Phys. Lett.* A **133** 433
Kovács L, Polgár K and Capelletti R 1987 *Cryst. Latt. Defects Amorph. Mater* **15** 115
Kovács L, Rebouta L, Soares J C and de Silva M F 1991 *Radiat. Eff. Defects Solids* **119–21** 445
Kovács L, Szaller Zs, Cravero I, Földvari I and Zaldo C 1990 *J. Phys. Chem. Solids* **51** 417
Novak A 1974 *Struct. Bonding* **18** 177
Petrosyan A K, Khachatryan R M and Sharoyan E G 1984 *Phys. Status Solidi* b **122** 725
de Rosendo Ma J, Arizmendi L, Cabrera J M and Agulló-López F 1986 *Solid State Commun.* **59** 499
Schirmer O F, Thiemann O and Wöhlecke M 1991 *J. Phys. Chem. Solids* **52** 185
Sweeney K L, Halliburton L E, Bryan D A, Rice R R, Gerson R and Tomaschke H E 1985 *Appl. Phys. Lett.* **45** 805
Zhang Q R and Feng X Q 1990 *Phys. Status Solidi* a **121** 429
Zhong G G, Jin J and Wu Z K 1980 *Proc. 11th Int. Quantum Electronics Conf.* (New York: IEEE) p 631